August 2026
Volume 2
Issue 3

DOI: 10.48308/ijce.2026.107748

Interdisciplinary Journal of Civil Engineering
Shahid Beheshti University

Effect of Single Friction Pendulum Isolator on Reduction of Drift Ratio in Compliance with FEMA P695

Authors:

Mohammad Ghoreishi[1], Mohammadjavad Hamidia[1,*], Nemat Hassani[1]

Abstract

This study investigates the effect of single friction pendulum (SFP) bearings on the maximum interstory drift of steel moment-resisting frames. Three two-dimensional models, representing 3-, 6-, and 9-story buildings, were examined in fixed-base and base-isolated configurations using OpenSeesPy. The bearings were selected through a simplified design procedure and modeled with nonlinear friction-pendulum elements, whereas the steel beams and columns were represented by elastic elements. Each configuration was subjected to the same 44 horizontal far-field earthquake components from the FEMA P695 suite. For every analysis, the largest absolute interstory drift ratio was extracted and compared with the corresponding fixed-base response. The mean record-wise reductions were 51.62%, 51.80%, and 55.59% for the 3-, 6-, and 9-story frames, respectively. All three isolated models also showed lower median peak drifts and smaller sample standard deviations. The paired record comparisons and distributions indicate a clear overall reduction in superstructure deformation, although the magnitude of that reduction varies with the earthquake component. These results demonstrate the potential of SFP bearings to improve drift control across the investigated steel frame configurations.

Keywords: Friction Pendulum Isolator, Interstory Drift, Base Isolation, Steel Frame, FEMA P695

1. Faculty of Civil, Water, and Environmental Engineering, Shahid Beheshti University, Tehran, Iran

*Corresponding Author: m_hamidia@sbu.ac.ir

1. Introduction

Interstory drift is a central measure of how a building deforms during earthquake shaking. Because adjacent floors generally move by different amounts, the relative horizontal displacement between them, divided by the story height, describes the local distortion of the frame. Excessive drift can damage partitions, glazing, cladding, and other nonstructural components while increasing deformation demands in structural members. For steel moment frames, whose lateral resistance depends largely on beam and column flexure, controlling this response is therefore an important part of seismic assessment. The ratio is especially informative because it provides a dimensionless measure of deformation, allowing stories with different heights to be compared using a common response scale. The maximum value over a response history is frequently used to summarize the severity of lateral deformation during a particular earthquake.

The distribution of drift along a building depends on its stiffness, mass, damping, and lateral-force-resisting system. In a conventional fixed-base steel frame, ground movement is transmitted through the supports, producing floor accelerations and relative displacements. The most highly deformed story may change from one earthquake to another, depending on the motion's frequency content and the building's dynamic properties. Examining several records consequently gives a more representative picture of the response than relying on a single excitation.

Seismic isolation changes the way this lateral motion reaches the superstructure by introducing a flexible, energy-dissipating interface near the foundation. A larger share of the overall movement can then occur in the isolation layer, allowing the floors above it to move more closely together and develop smaller relative displacements. Successful implementation still requires adequate restoring force, energy dissipation, and displacement capacity, so the benefit is best evaluated through the response quantities most relevant to the design objective. The resulting displacement is distributed differently between the foundation interface and the floors above it. The aim in this work is to determine whether that redistribution produces a measurable decrease in superstructure drift, rather than to evaluate isolation efficiency from bearing movement alone.

The single friction pendulum bearing is an established example of this approach. Its slider travels over a concave surface, where sliding friction dissipates energy and the surface curvature produces a gravity-driven restoring action. The underlying mechanism was introduced by Zayas et al. (1990) and examined experimentally by Mokha et al. (1991). The combination of frictional nonlinearity and restoring stiffness provides a practical basis for studying drift reduction in steel frames whose members are represented elastically.

Seismically isolated buildings may be evaluated in terms of bearing travel, floor acceleration, local force, structural damage, or collapse performance. Here the emphasis is specifically on

peak interstory drift. For each earthquake component, a fixed-base frame and its SFP-isolated counterpart are analyzed under the same input, and the difference in their maximum drift ratios is expressed relative to the fixed-base result. Repeating this paired comparison over the ground-motion suite shows both the overall reduction and its variation from record to record. Using the same ground-motion component in the two models removes differences in excitation from each individual comparison. Although the frame properties change when the isolation layer is introduced, the paired response values can still be interpreted clearly because they correspond to the same imposed history.

The numerical examples consist of planar steel frames with 3, 6, and 9 stories, developed with reference to the Steel Project. The configurations provide a documented starting point for steel moment-frame research, although the present six-story model is an adapted intermediate-height frame. The results therefore refer to the specific OpenSeesPy models examined here.

The selected seismic inputs are 44 horizontal components from the FEMA P695 far-field ground-motion suite (Federal Emergency Management Agency [FEMA], 2009). Identical components were used for each fixed-base/isolated pair, permitting consistent record-level comparisons. After reviewing relevant research, the paper describes the structural and isolation models, explains the drift measures, and discusses the mean, median, and variability of the observed reductions.

2. Literature Review

The principles of base isolation are well documented in earthquake engineering literature. By modifying the dynamic properties of the structure, the isolation layer can reduce the deformation transmitted to the upper frame. Naeim and Kelly (1999) describe both the mechanics of isolation devices and their practical design, including the relationship between equivalent-linear design procedures and more detailed response-history models. These complementary approaches are relevant to the present study, where simplified bearing design is followed by numerical earthquake analysis. The equivalent-linear description is particularly convenient for selecting preliminary isolation properties, since it condenses the main force–displacement characteristics into a period and damping value. The subsequent nonlinear analysis can then examine how those selected properties respond to the complete sequence of acceleration reversals.

Reviews by Buckle and Mayes (1990), Jangid and Datta (1995), and Warn and Ryan (2012) trace the development of seismic isolation and its application to buildings. A common theme is that performance depends on the interaction among device behavior, superstructure characteristics, and the imposed motion. That interaction also provides the context for comparing drift responses in frames of different heights.

In the friction pendulum concept described by Zayas et al. (1990), the sliding surface geometry determines part of the restoring force through the supported weight. For otherwise comparable bearings, increasing the curvature radius reduces the gravity-related lateral stiffness, while friction both opposes sliding and dissipates energy. These coupled mechanisms explain how an SFP bearing can modify the period and deformation response of the supported frame.

Subsequent analytical studies developed more detailed representations of the same sliding mechanism. Almazán et al. (1998) addressed modeling issues associated with friction pendulum motion, and Almazán and De la Llera (2002) proposed an analytical formulation for structures with frictional pendulum isolators. Together, these investigations provide a basis for combining simplified design calculations with nonlinear simulations that capture the response of the sliding interface.

Experimental work has provided an important complement to analytical modeling. Mokha et al. (1991) investigated friction pendulum isolation in a multistory test structure, showing how the response changes under motions with different frequency characteristics. Their findings also drew attention to bearing displacement and residual movement. The present numerical comparison focuses on a related effect: how the sliding layer changes deformation within the floors above it.

The frictional behavior of sliding interfaces was examined in the tests by Mokha et al. (1990) and in the modeling study by Constantinou et al. (1990). Mosqueda et al. (2004) subsequently characterized friction pendulum bearings subjected to multiple excitation components. These contributions reinforce the importance of representing the isolator as a distinct nonlinear component rather than assigning its behavior to the elastic steel members.

Simplified isolation design commonly describes the system through an effective period and an equivalent damping ratio evaluated at a selected displacement. This representation connects the bearing's friction and curvature to the expected dynamic response, as discussed by Naeim and Kelly (1999). Response-history analysis then resolves the time-dependent sliding behavior, including changes in friction force direction and the influence of individual acceleration pulses. In effect, the design quantities are associated with an assumed response amplitude. Evaluating the resulting system under individual earthquake histories is therefore a natural continuation of the design process, especially when the objective is to compare maximum structural deformation.

Kelly (1999) examined how damping affects isolation response, including the possible trade-off between reducing bearing motion and changing the demands in the superstructure. Fenz and Constantinou (2006) extended the discussion to double-concave bearings. Although their configuration differs from the single-surface SFP device studied here, the work illustrates the broader influence of sliding geometry on seismic response.

Numerical analysis makes it possible to evaluate the same frame and earthquake component with different support conditions. OpenSees provides a framework for nonlinear structural simulation (McKenna, 2011), and its Python interface is described by Zhu et al. (2018). In this work, the singleFPBearing element represents frictional sliding and curvature-related restoring action, while elastic beam-column elements describe the steel superstructure.

Ground-motion selection also affects the interpretation of response statistics. Shome et al. (1998) examined the influence of earthquake records on structural response estimates and highlighted record-to-record differences. Variations in amplitude, duration, and frequency content can change maximum drift even when the structural model is unchanged; applying identical components to both support conditions therefore creates a consistent basis for the paired comparisons. The direct pairing is particularly important for percentage reductions, since the denominator is the response of the corresponding fixed-base frame to the very same excitation. Without that matching, the calculated difference would combine the effects of support condition and record selection.

The Steel Project supplied widely studied steel moment-frame configurations and related investigations following the Northridge earthquake. Their documented geometry and member properties provide a valuable point of departure for numerical studies. Because individual studies may adapt the original configurations, the frame dimensions and modeling assumptions adopted here are stated explicitly in the next section.

Other numerical investigations have considered friction pendulum isolation in steel-frame applications. Jangid (2005) examined response under near-fault motions, while Matsagar and Jangid (2008) addressed isolation in structural retrofit. Deringöl and Güneyisi (2019) studied 3-, 6-, and 9-story steel frames equipped with friction pendulum bearings and considered the effect of bearing properties on seismic behavior. Although the configurations and analytical choices differ from those used here, these studies provide relevant background for interpreting changes in drift demand.

More recent work has broadened the evaluation of isolated buildings beyond drift control. Kitayama and Constantinou (2018) investigated collapse performance, and Kitayama and Cilsalar (2022) considered seismic losses. Those studies demonstrate the range of available performance measures; the present analysis concentrates instead on the peak drift response of three frames under 44 paired far-field components.

Taken together, previous studies explain the mechanical basis of friction pendulum isolation and the importance of variability among earthquake records. Building on that foundation, this work presents the paired maximum drifts for fixed-base and isolated configurations and compares their means, medians, and sample standard deviations. The combination of individual and summary results makes the observed changes easier to interpret. The approach is intended to give readers more than a single measure of effectiveness: the individual bars show the

demand caused by each motion, the medians describe the central response, and the standard deviations indicate how widely the response changes within the selected suite.

3. Structural Models and Isolation System

3.1. Building Configurations

Three planar steel moment-resisting frames were modeled, representing buildings with 3, 6, and 9 stories. Each was analyzed with fixed column bases and with an SFP isolation layer placed below an otherwise corresponding superstructure. The paired configurations allow the influence of the isolation system on relative floor displacement to be examined under identical earthquake components. The comparison is organized by building height, with the two support conditions forming a pair for every earthquake input. This arrangement keeps the numerical procedure consistent across models while allowing the geometry and member properties of the three frame configurations to remain distinct.

The three-story frame comprises three 30-ft bays with a story height of 13 ft and uses section properties based on a low-rise configuration. The six-story frame, treated as an adapted intermediate-height model, has three 24-ft bays and 12.5-ft stories. The nine-story frame comprises four 30-ft bays with a 13-ft story height. These dimensions correspond to the OpenSeesPy models developed for the analysis.

The beam and column properties were assigned by cross-sectional area and moment of inertia, following the member schedules in the numerical models. An elastic modulus of 29,000 ksi was adopted for steel, and all computations used consistent inch–kip–second units for geometry, mass, weight, stiffness, and acceleration.

Gravity loading was established before dynamic excitation so that the frame forces and the axial loads carried by the bearings were represented at the start of each response history. A base slab was included above the isolation interface; its lateral displacement formed the lower reference for first-story drift in the isolated frames. Thus, the response measure describes relative deformation of the superstructure rather than roof travel relative to the ground. The distinction between frame drift and absolute base movement is essential in an isolation study. Otherwise, the first-story response could include translation across the bearings and would no longer describe the same deformation mechanism used to characterize the fixed-base superstructure. Table 1 summarizes the frame geometry. The labels A, B, and C identify the three models in this study. Because their bay arrangements, member properties, weights, and isolation designs differ, the comparisons characterize each complete frame configuration rather than the isolated influence of story count.

Table 1. Geometry of the steel frame models implemented in OpenSeesPy.

Model	Stories	Bays	Bay length	Story height	Description
A	3	3	30 ft	13 ft	low-rise frame
B	6	3	24 ft	12.5 ft	Adapted intermediate frame
C	9	4	30 ft	13 ft	mid-rise frame

3.2. Representation of the Steel Superstructure

Beams and columns were represented by the OpenSees elasticBeamColumn element, using the assigned area, second moment of area, and elastic modulus. This formulation provides a consistent linear-elastic superstructure for the fixed-base and isolated cases, allowing the influence of the nonlinear bearing layer on drift response to be examined directly. The same member idealization is retained within each fixed-base/isolated pair. Differences in peak drift can therefore be discussed in relation to the change in support behavior while maintaining the prescribed elastic properties of the superstructure.

A P-Delta geometric transformation was assigned to the columns to account for the influence of axial loads on equilibrium in the laterally displaced configuration. Nodes on each floor were linked in the horizontal direction, and the floor weights supplied the corresponding lumped masses. The resulting two-dimensional models capture the principal in-plane translation of each story.

The isolated configurations included a bearing at each modeled support position and a separate set of nodes for the moving base slab. The fixed-base counterparts retained the direct support restraints. Both configurations were subjected to horizontal excitation in the frame plane, keeping the comparison focused on the deformation of the modeled lateral system.

Peak interstory drift ratio was selected as the principal response measure because it directly represents relative movement between adjacent floors. It allows a consistent comparison of the superstructure deformation in the two support conditions and provides the basis for the statistical evaluation presented in Section 5.

3.3. Simplified Design of the Single Friction Pendulum Bearings

The SFP bearings were designed by a simplified procedure based on effective dynamic properties at a selected displacement. The approach represents the isolation layer through an equivalent oscillator, linking frictional resistance and surface curvature to an effective period and damping ratio. The resulting bearing designs were then implemented in the nonlinear numerical models, with each frame assigned a system appropriate to its configuration. The

simplified model is used at the design stage to relate the desired displacement level to a representative force–displacement response. After the design properties are selected, the bearing element in OpenSeesPy provides the nonlinear sliding behavior during the earthquake analyses.

The lateral resistance of a friction pendulum bearing combines a friction component associated with the supported vertical load and a gravity-related restoring component produced by movement along the curved surface. At the selected design displacement Δ, these contributions define the effective secant stiffness; combining that stiffness with the supported mass gives the corresponding effective frequency and period. In the equivalent representation, the effective stiffness depends on the displacement selected for evaluation rather than being a single constant for all motion amplitudes. This displacement dependence motivates the sequence of effective-period, effective-damping, and spectral-displacement calculations that follows.

The effective period T_{eff} can be written as follows:

$$T_{eff}=2\pi\sqrt{\frac{1}{\mu g/\Delta+g/R_{eff}}} \tag{1}$$

In Equation (1), μ denotes the friction coefficient, g the acceleration of gravity, Δ the design displacement, and R_{eff} the effective radius of the sliding surface. A larger displacement reduces the relative contribution of friction to secant stiffness, while a larger curvature radius reduces the geometric restoring stiffness. The resulting effective period represents the bearing response at the selected design displacement. The terms in the denominator of Equation (1) indicate the contributions of friction and curvature to the effective horizontal restoring action. Their combined effect determines the period used in the simplified spectral calculation at the adopted design displacement. Energy dissipation through friction is expressed in the equivalent-linear design approach as an effective damping ratio, calculated for the selected displacement using Equation (2):

$$\xi_{eff}=\min\left\{\frac{2}{\pi}\left[\frac{\mu}{\mu+\Delta/R_{eff}}\right],\ 0.30\right\} \tag{2}$$

The upper bound of 0.30 in Equation (2) caps the equivalent damping ratio in the simplified calculation. This value describes energy dissipation in the isolation system and is separate from the viscous damping assigned to the steel frame, since the nonlinear bearing itself represents frictional energy loss. A response spectrum drawn for 5% damping may be adjusted when a different effective damping ratio is used. The damping modification factor β was calculated by:

$$\beta=\left(\frac{\xi_{eff}}{0.05}\right)^{0.3} \tag{3}$$

The factor β adjusts the five-percent-damped spectrum to the effective damping of the isolated system. Using the convention in Equation (3), the spectral ordinate at the effective period is divided by β before the displacement demand is evaluated, providing a link between the equivalent-linear design model and the seismic input. The adjustment changes the spectral demand associated with the equivalent isolation oscillator and provides a displacement estimate for the next step of the procedure. It is the calculated displacement, rather than the damping factor alone, that is compared with the assumed design displacement. The damping-adjusted spectral acceleration at the effective period is calculated from the corresponding five-percent-damped spectrum as follows:

$$S_a\left(T_{eff},\xi_{eff}\right)=\frac{S_{a,5\%}(T_{eff})}{\beta} \tag{4}$$

The corresponding spectral displacement was then calculated from the acceleration-displacement relationship for an equivalent oscillator:

$$S_D=\frac{S_a T_{eff}^2}{4\pi^2} \tag{5}$$

Equation (5) requires spectral acceleration in physical acceleration units; when the spectrum is expressed in multiples of g, the ordinate is first converted accordingly. The resulting displacement S_D is compared with the assumed design displacement Δ, and the effective properties can be updated until the simplified calculation is consistent. Iterating between the effective properties and the spectral demand provides a straightforward way to reach a compatible design estimate. The same physical quantities are then represented in the nonlinear bearing element when the building is subjected to the individual earthquake histories.

The bearings were selected separately for the three frame configurations, and their design values were carried into the OpenSeesPy models. The present analysis emphasizes the resulting drift response rather than a parametric investigation of individual bearing properties.

After the design-stage properties were established, the nonlinear bearing response was represented by the OpenSeesPy singleFPBearing element. A Coulomb friction model described sliding resistance, while the concave interface supplied the geometric restoring action; the remaining required directions were assigned suitable material models (McKenna, 2011; Zhu et al., 2018). This formulation captures the principal sliding behavior within the response-history analysis. Unlike an equivalent spring with a single constant stiffness, the bearing element can respond differently as the direction and magnitude of sliding change. This behavior is relevant to a record-by-record investigation because the acceleration histories do not produce identical displacement cycles.

3.4. Damping and Gravity Load Treatment

The upper steel frames were assigned 5% nominal first-mode damping through a stiffness-proportional Rayleigh term in the OpenSeesPy models, with the mass-proportional term set to zero. In the isolated configurations, this damping was applied to the superstructure, while energy dissipated by sliding was represented directly in the nonlinear bearing element.

Static gravity loading preceded the horizontal response-history analysis, establishing the axial forces that govern bearing friction. After the gravity state was held constant, the acceleration history was applied, and the time-stepping solution followed the changing displacement response. The recorded motions contain changes in direction, strong-motion pulses, and intervals that can influence whether a bearing sticks or slides. While the simplified equations establish design-stage properties, the response-history calculations determine the maximum interstory drifts examined in the following sections.

4. Ground-Motion Analysis and Drift Measures

4.1. FEMA P695 Far-Field Suite

The seismic input consists of 44 horizontal far-field components from the FEMA P695 ground-motion suite, which is presented within a broader framework for evaluating seismic performance factors (FEMA, 2009). Here, the records provide a common set of earthquake excitations for comparing maximum interstory drift in fixed-base and SFP-isolated steel frames. The suite includes different events and recording conditions, which broadens the range of excitation characteristics applied to each frame. By keeping the input set common across all six configurations, the comparison emphasizes changes in response associated with the modeled support condition.

The 44 components form 22 pairs of horizontal earthquake records. Each component was applied to both support conditions for the 3-, 6-, and 9-story frames, with its time increment obtained from the motion-file information and horizontal acceleration introduced through OpenSees UniformExcitation. Retaining the same record order across the models facilitates direct comparison of the resulting drift demands.

The response-history dataset includes components from Northridge, Düzce, Hector Mine, Imperial Valley, Kobe, Kocaeli, Landers, Loma Prieta, Manjil, Superstition Hills, Cape Mendocino, Chi-Chi, San Fernando, and Friuli. Pairs from a given station represent different horizontal directions, whereas components from different events extend the range of motion characteristics. The statistical summaries treat the 44 components as observations while recognizing that two recordings from the same station belong to the same earthquake event. In the tables and plots, the component number serves as a common identifier rather than a ranking

by earthquake intensity or resulting drift. This ordering makes it possible to inspect the two horizontal directions from a recording station alongside the responses of the other components.

Presenting results component by component retains information that would be lost in a single average reduction. The paired bars display the different demands produced by horizontal components from the same station and identify records for which the isolated frame still experiences comparatively large drift.

4.2. Nonlinear Response-History Procedure

Each transient analysis began from the gravity-loaded configuration. Horizontal acceleration was then introduced through a Newmark integration scheme with iterative equilibrium solution, and nodal displacements were tracked throughout the response history. The numerical model was reinitialized for each earthquake so that every run began from the same prescribed initial conditions. The computed displacements were evaluated as time-dependent responses rather than as static lateral-load results. At each step, the maximum story drift encountered so far was updated, so the final reported quantity represents the most severe relative floor deformation in that run.

For fixed-base frames, interstory drift was obtained from the difference in lateral displacement between successive floors. In the isolated models, the first-story reference was the moving base slab, separating deformation of the steel frame from translation across the bearing layer. This definition ensures that the paired results represent comparable superstructure response quantities.

For each earthquake component, the OpenSeesPy models tracked the largest absolute drift at each story and retained the maximum across the full building. One peak value was therefore obtained for every fixed-base or isolated run. With three frame heights and 44 earthquake components, the response-history dataset contains 132 paired comparisons, corresponding to 264 peak drift values. The resulting data structure is compact but preserves the essential pairing between the support conditions. It also allows statistics to be calculated separately for each frame height without combining observations from structurally different models.

The values were assembled by frame height and earthquake component, with each pair containing the fixed-base maximum drift and the corresponding SFP-isolated maximum drift. This organization supports direct calculation of the record-wise reduction percentage and a consistent comparison across all three configurations.

4.3. Peak Interstory Drift Ratio

The interstory drift ratio at time t is the absolute difference between horizontal displacements at adjacent floor levels divided by the corresponding story height. For each frame and

earthquake component, the peak ratio is obtained by taking the maximum over all stories and analysis time steps:

$$IDR_{max}=\max_{i,t}\left\{\frac{|u_i(t)-u_{i-1}(t)|}{h_i}\right\} \quad (6)$$

In Equation (6), $u_i(t)$ and $u_{i-1}(t)$ are the lateral displacements of successive floors, and h_i denotes the height of story i. For the first story in an isolated model, the lower displacement corresponds to the moving isolation slab. The ratio is dimensionless and is multiplied by 100 when reported as a percentage in the tables and figures.

The drift reduction for an earthquake component is measured relative to its fixed-base response:

$$\text{Reduction (\%)}=100\left[1-\frac{IDR_{\max,SFP}}{IDR_{\max,FB}}\right] \quad (7)$$

Equation (7) gives a positive value when the isolated drift is smaller than the fixed-base drift and zero when the responses coincide. The reduction is calculated separately for each component, then averaged across the 44 paired results for each frame. This mean of individual percentages differs from the percentage obtained by comparing the two group means. This distinction in averaging is maintained throughout the Results section so that the reported mean reduction has one consistent meaning. The numerical summaries are based on 44 values for each height, each obtained from a fixed-base/isolated pair.

The distinction matters when the magnitude of the fixed-base response varies substantially among records. The ratio of the group means gives greater influence to components producing large absolute drift, whereas the mean record-wise reduction gives equal weight to each component's percentage. Reporting both measures clarify how the summaries were obtained.

4.4. Median and Standard Deviation

The median describes the central value of the peak-drift distribution. With 44 observations, it is the average of the 22nd and 23rd values after sorting; compared with the mean, it is less sensitive to unusually large responses. It therefore provides an additional view of the typical drift observed within the earthquake suite. When the distribution is skewed by a few large drift demands, the median can remain close to the values produced by most of the records. Comparing the median before and after isolation therefore adds perspective to the average reduction.

The sample standard deviation characterizes the spread of the 44 peak drifts around their mean, using $n - 1$ in the denominator for $n = 44$. It was calculated separately for the fixed-base and isolated responses at each height, so the resulting values describe the dispersion of drift demand rather than dispersion of the percentage reduction. Together, the mean, median, and standard

deviation summarize the magnitude, central tendency, and spread of the response distribution. These statistics complement the paired record charts, which retain the component-specific differences concealed by a single summary measure.

5. Results and Discussion

5.1. Main Drift Statistics

Table 2 summarizes the peak interstory drift statistics obtained from the response-history dataset. Mean fixed-base and isolated drifts were 1.317% and 0.528% for the three-story frame, 1.110% and 0.461% for the six-story frame, and 1.051% and 0.405% for the nine-story frame. Across all three heights, the isolated systems exhibited lower average drift demand. These means are based on the maximum value reached anywhere in each modeled superstructure during an earthquake history. They therefore summarize building-level peak demand for the selected records rather than a time-averaged drift or an average over stories.

Table 2. Peak interstory drift ratio statistics for the 44 records in each frame configuration.

Stories	Condition	Mean (%)	Median (%)	Std. dev. (%)	Min (%)	Max (%)
3	Fixed-base	1.317	1.118	0.713	0.353	3.499
3	SFP-isolated	0.528	0.527	0.104	0.314	0.867
6	Fixed-base	1.110	1.030	0.501	0.258	2.294
6	SFP-isolated	0.461	0.427	0.127	0.245	1.040
9	Fixed-base	1.051	1.004	0.547	0.243	2.968
9	SFP-isolated	0.405	0.354	0.209	0.194	1.586

The medians follow the same trend, decreasing from 1.118% to 0.527% in the three-story frame, from 1.030% to 0.427% in the six-story frame, and from 1.004% to 0.354% in the nine-story frame. Their reduction indicates that the overall benefit extends to the center of the response distributions rather than being driven only by a few large fixed-base values.

The maximum fixed-base drift across the 44 records was 3.499%, 2.294%, and 2.968% for the three frame heights, respectively, compared with maximum isolated values of 0.867%, 1.040%, and 1.586%. Because isolation changes the dynamic characteristics of the system, the record governing the fixed-base maximum need not govern the isolated maximum as well.

Averaging the percentage reduction computed from Equation (7) over all components gives 51.62% for the three-story model, 51.80% for the six-story model, and 55.59% for the nine-story model. The first two results are particularly close, whereas the nine-story frame shows a somewhat larger mean reduction. These differences reflect the response of each complete frame and bearing configuration. The differences among the three mean reductions are relatively modest compared with the variation observed among individual components. This motivates the closer examination of the record-wise reduction ranges and frequencies presented in Table 3.

Table 3. Record-wise percentage drift reductions and number of records above selected reduction levels.

Stories	Mean (%)	Median (%)	Min (%)	Max (%)	≥25%	≥50%	≥75%
3	51.62	53.35	6.01	83.44	39	25	4
6	51.80	55.51	4.99	81.10	38	27	4
9	55.59	56.77	9.56	81.80	42	27	5

Table 3 shows the distribution of record-wise reductions. At least 25% reduction was achieved in 39 of 44 components for the three-story frame, 38 for the six-story frame, and 42 for the nine-story frame; the corresponding counts at the 50% threshold were 25, 27, and 27. These values are observed frequencies within the analyzed suite. Percentages in the table follow the entries in the response-history dataset, so small differences can appear when using rounded drift values for an independent recalculation. The threshold counts describe how often a specified level of improvement appeared in the finite record set. They complement the mean and median reductions by showing the frequency of moderate and larger improvements without assigning a formal probability to events outside the analyzed suite.

At the 75% threshold, four components met or exceeded the level in each of the three- and six-story frames, compared with five in the nine-story frame. The wide range of individual reductions shows why the approximate 50% group average cannot describe every earthquake component: some paired responses are close, whereas others differ markedly. These contrasts are visible in Figure 1.

5.2. Record-By-Record Drift Comparisons

Figure 1 combines the three record-by-record comparisons in a common multi-panel layout. Panels (a), (b), and (c) correspond to the 3-, 6-, and 9-story frames, respectively, with two neighboring bars for each of the 44 horizontal components. Blue denotes the fixed-base peak drift and orange the SFP-isolated peak drift. Keeping the component order identical across panels allows the three frame responses to be examined against the same sequence of motions. A larger gap between two neighboring bars identifies a record for which the isolated model

developed much lower drift than its fixed-base counterpart. Conversely, nearly equal bar heights identify components for which the measured improvement was more modest. More details are presented in Table A1.

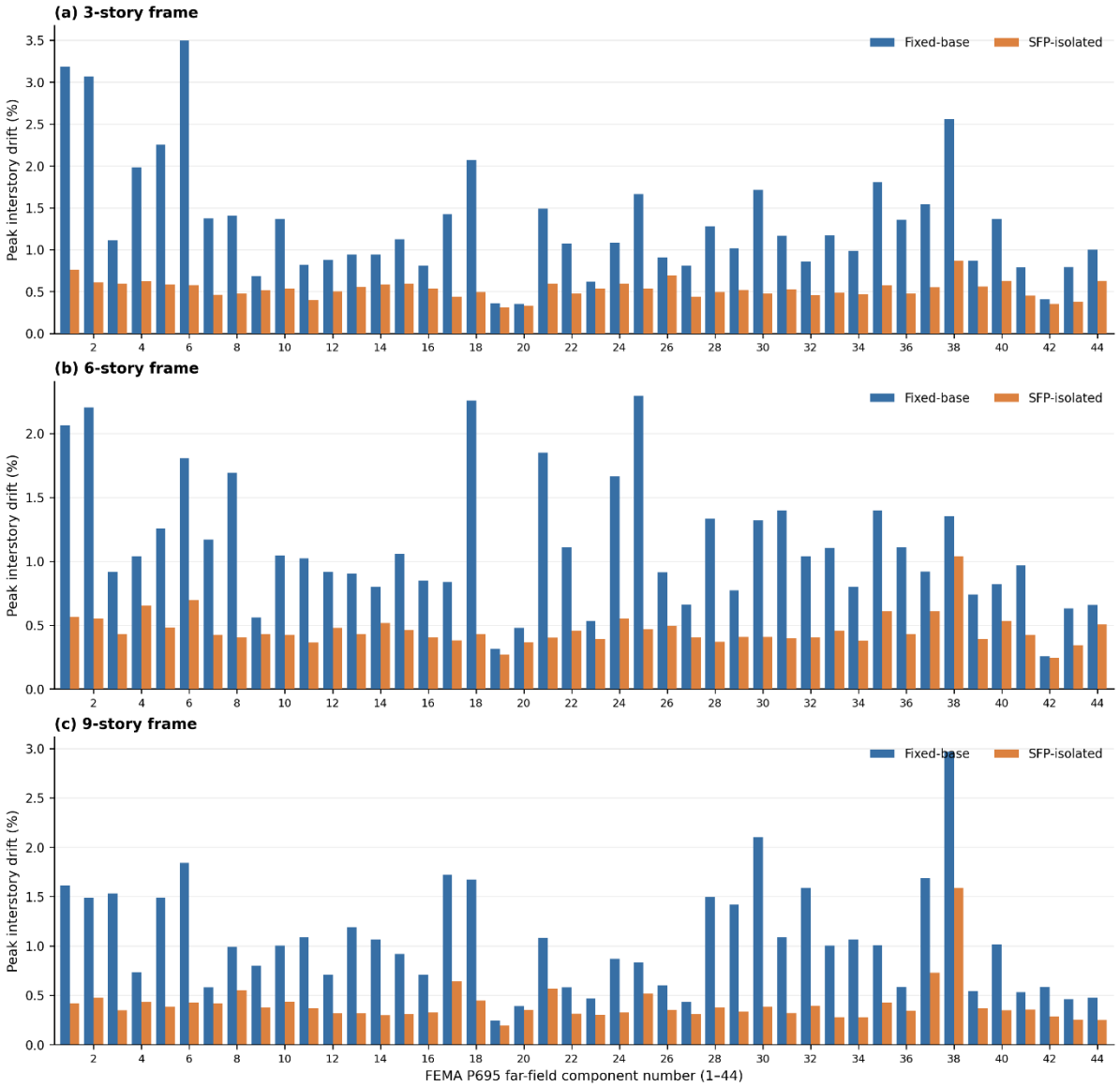


Figure 1. Peak interstory drift ratio under 44 FEMA P695 far-field components: (a) 3-story, (b) 6-story, and (c) 9-story frames; paired fixed-base and SFP-isolated bars

Lower isolated peaks are apparent throughout the panels, particularly in the three- and six-story models, where the isolated values occupy a narrower absolute range. The bars also reveal substantial differences among earthquake components, emphasizing the importance of considering both the paired demands and the statistical summaries.

For the three-story frame in Figure 1(a), the largest reduction occurred under record 6, the Düzce motion recorded at Bolu in the 090 direction. Peak drift decreased from 3.499% in the

fixed-base model to 0.579% with isolation, a record-wise reduction of 83.44%. The remaining components show varying degrees of improvement, with the isolated values generally more closely grouped.

At the other end of the three-story range, record 20—the Kocaeli component recorded at Arçelik in the 090 direction—produced fixed-base and isolated peak drifts of 0.353% and 0.332%, respectively, corresponding to a 6.01% reduction. In this case, the relatively small initial drift also limits the absolute difference between the two bars. For the three-story model, 25 of the 44 components achieved at least a 50% reduction. Figure 1(a) therefore captures both the broad improvement and the variation around the average, which is also reflected in the smaller isolated standard deviation.

In the six-story frame shown in Figure 1(b), the largest percentage reduction was obtained under record 18, a Kocaeli motion recorded at Düzce in the 270 directions. Peak drift fell from 2.260% in the fixed-base configuration to 0.427% after isolation, giving an 81.10% reduction. The record governing this extreme differs from the three-story case, reflecting the dependence of the response on the combined frame and motion characteristics.

The smallest six-story reduction was 4.99%, under record 42 from the San Fernando event at the LA Hollywood Storage station, where the fixed-base and isolated peaks were 0.258% and 0.245%. By contrast, record 38 from Chi-Chi produced the largest isolated peak drift of 1.040%, indicating that the sliding layer still experiences component-dependent demands. Across the six-story records, 38 components achieved at least 25% reduction, 27 achieved at least 50%, and four achieved at least 75%. The distribution therefore shows a consistent direction of improvement alongside considerable variation in its magnitude.

Figure 1(c) presents the nine-story results. Record 38, the Chi-Chi CHY101 component in the N direction, produced the largest peak drifts in both support conditions: 2.968% for the fixed-base frame and 1.586% for the isolated frame. Its reduction was 46.57%, while the greatest record-wise improvement of 81.80% occurred under record 30, a transverse component of the Manjil event recorded at Abbar. This record is also notable because it produces great absolute demands in both configurations. The paired comparison shows that the isolated drift can remain substantial for an individual component even when the overall percentage reduction is favorable. The smallest nine-story reduction, 9.56%, occurred under record 20 from Kocaeli at Arçelik in the 090 direction. Nevertheless, 42 components achieved reductions of at least 25%, and 27 achieved at least 50%, indicating that the response improvement extended across most of the examined motions.

The isolated nine-story results have a broader high-response tail than the isolated three-story results, even though the overall mean isolated drift is lower. This feature becomes clearer when the median and standard deviation are considered together in the following subsections.

5.3. Median Peak-Drift Distributions

The median offers a complementary description of peak drift, particularly when individual ground motions generate unusually large responses. Figures 2–4 combine the fixed-base distribution in panel (a) with the SFP-isolated distribution in panel (b) for the 3-, 6-, and 9-story models. A dashed vertical line identifies the median in each panel, enabling direct comparison of the central drift level and the frequency distribution. The two-panel layout preserves the shape of each distribution while keeping the support conditions visually distinct. Comparing the locations of the dashed median lines indicates the shift in the central response without requiring the reader to compare several separate figures.

Each histogram summarizes the 44 building-level maximum interstory drift values for the indicated configuration. The horizontal axis therefore represents peak drift demand for an entire response history rather than the distribution of drift over individual floors.

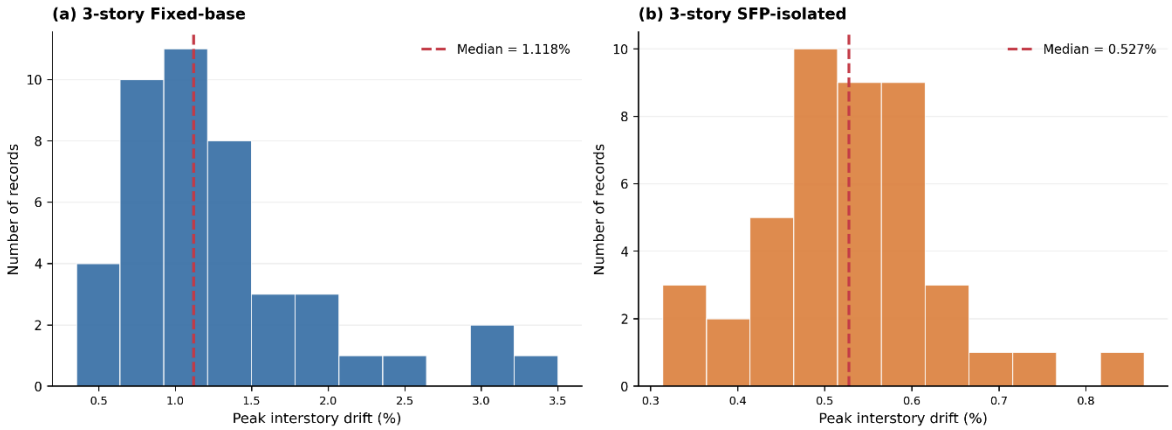


Figure 2. Distribution and median of peak interstory drift for the 3-story frame: (a) fixed-base and (b) SFP-isolated

For the three-story frame, the median peak drift decreases from 1.118% in the fixed-base condition to 0.527% after isolation. Because the bearing layer changes the dynamic response, the relative ordering of individual component demands can also change; nevertheless, the central value of the isolated distribution lies substantially below that of the fixed-base distribution. The isolated three-story histogram is more tightly concentrated, consistent with its markedly smaller sample standard deviation. Together, the two panels describe the shift in both the central drift level and the observed range over the 44 components.

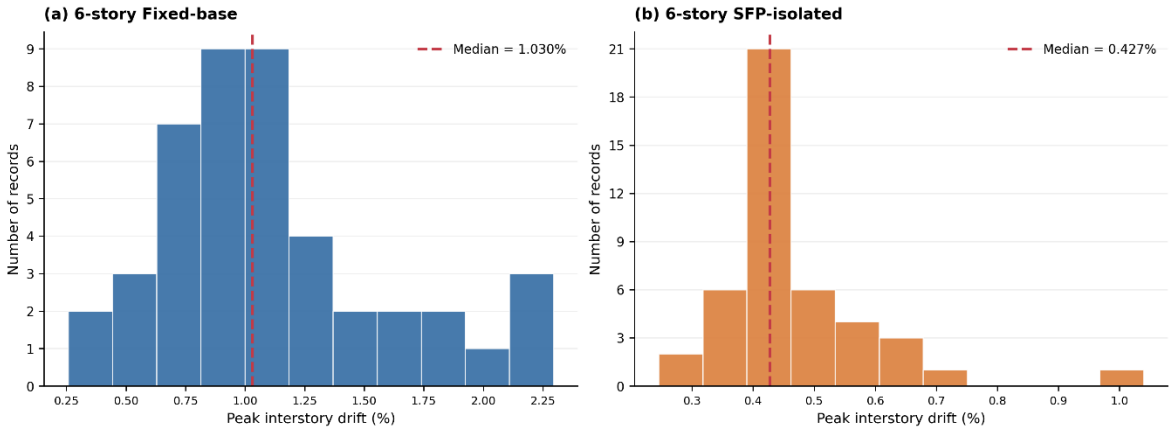


Figure 3. Distribution and median of peak interstory drift for the 6-story frame: (a) fixed-base and (b) SFP-isolated

Figure 3 shows a decrease in the six-story median from 1.030% for the fixed-base frame to 0.427% for the isolated frame. The fixed-base histogram spans a wider interval, while much of the isolated distribution lies near its lower peak values. A small number of larger isolated responses, including the Chi-Chi component discussed above, remains visible. Although the three- and six-story frames have nearly identical mean record-wise reductions, their absolute medians differ. This comparison illustrates how two models may obtain similar relative benefits while retaining distinct stiffness, mass, and peak-drift levels.

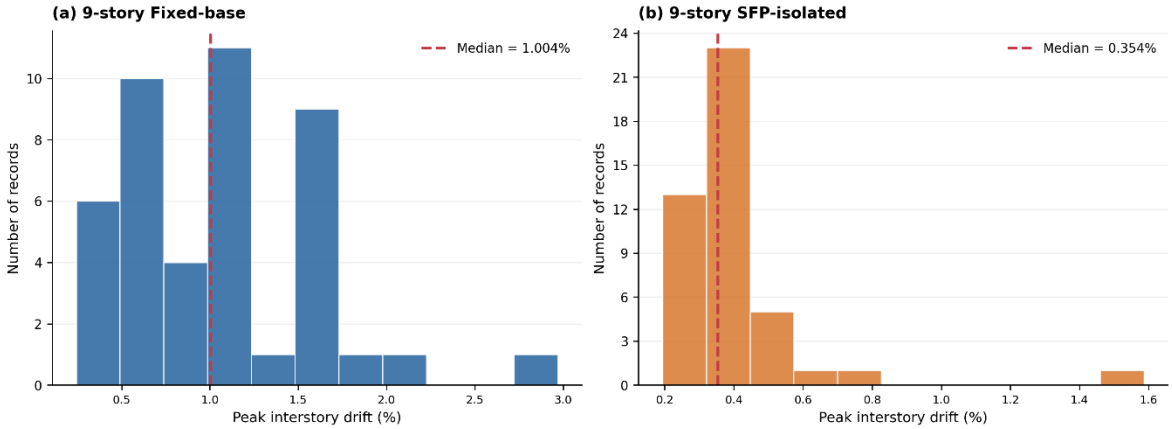


Figure 4. Distribution and median of peak interstory drift for the 9-story frame: (a) fixed-base and (b) SFP-isolated

In Figure 4, the nine-story median decreases from 1.004% to 0.354% following the introduction of SFP isolation. This shift agrees with the larger mean record-wise reduction reported for the nine-story configuration. The result reflects the combined properties of that particular frame and its separately designed isolation system.

The isolated nine-story histogram contains a pronounced upper tail: record 38 produces a peak above 1.5%, whereas most components give substantially smaller values. The median describes the typical level without being dominated by this extreme, while the standard deviation captures its influence on the spread.

5.4. Standard Deviation and Record-To-Record Variation

Figure 5 compares the sample standard deviation of peak drift across all three heights in a three-panel arrangement. Panels (a), (b), and (c) correspond to the 3-, 6-, and 9-story models, and each displays the fixed-base and isolated results on the same vertical scale. This arrangement highlights changes in absolute record-to-record variability. The common scale also avoids exaggerating or obscuring differences among frame heights through changes in axis limits. Each panel therefore provides a consistent view of the absolute dispersion associated with its own fixed-base and isolated results.

The standard deviations are expressed in percentage points of drift. Their decrease after isolation indicates a narrower absolute spread, although relative variability must also be considered in relation to the corresponding mean. The median distributions provide additional context for the high-response components, especially in the nine-story case.

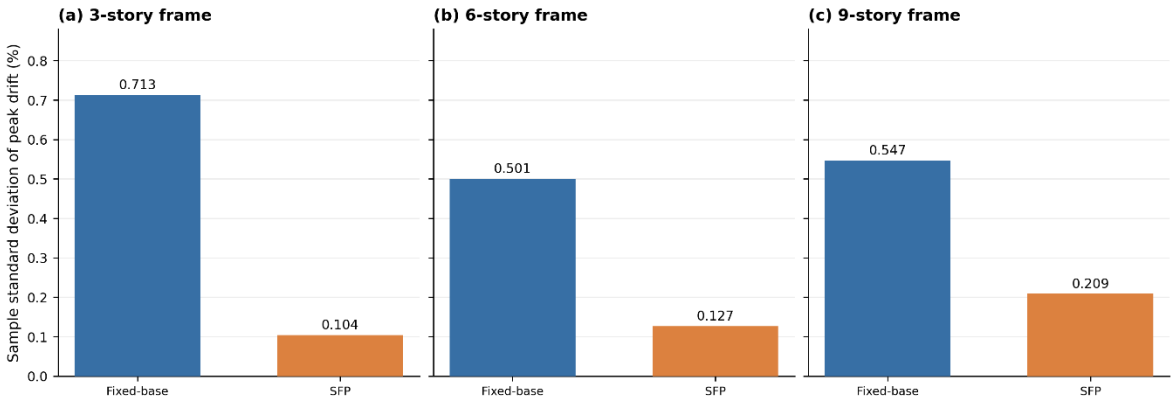


Figure 5. Sample standard deviation of peak interstory drift for (a) 3-story, (b) 6-story, and (c) 9-story frames, comparing fixed-base and SFP-isolated cases

For the three-story frame, the sample standard deviation decreases from 0.713 to 0.104 percentage points with isolation. The pronounced change matches the narrower isolated distribution in Figure 2 and indicates that the peak drifts are more closely clustered across the examined records. The six-story standard deviation decreases from 0.501 to 0.127 percentage points. Although the absolute spread is smaller after isolation, record 38 contributes a relatively large isolated response, underscoring the importance of reading the dispersion statistic alongside individual record results.

For the nine-story model, the corresponding values are 0.547 and 0.209 percentage points. Its reduction in absolute spread is smaller, relative to the original value, than in the three-story case. The isolated nine-story frame also shows more dispersion than the other isolated models despite having the lowest mean peak drift.

All three isolated configurations have smaller sample standard deviations than their fixed-base counterparts under the selected 44 components. This pattern, considered with the changes in mean and median response, supports the observed improvement in drift control while retaining the record dependence apparent in Figure 1.

5.5. Interpretation of the Isolation Benefit

The reduction in interstory drift is consistent with the altered path by which earthquake-induced movement reaches the upper frame. In the fixed-base condition, the members accommodate lateral deformation directly, whereas the isolated arrangement permits a portion of the movement to occur through sliding in the bearing layer. Friction dissipates energy, and the curved surface provides restoring action, together limiting relative motion between adjacent floors. For a given earthquake, these actions alter the relative contribution of the isolation layer and the upper frame to the overall lateral movement. The resulting peak drift provides a direct measure of how that change in deformation distribution affects the steel superstructure.

Because the ground motions differ in duration, frequency characteristics, and acceleration history, the magnitude of the isolation benefit varies among components. The fixed-base and isolated systems also have different effective dynamic properties, so a motion that strongly excites one may act differently on the other. The paired comparisons in Figure 1 are consistent with this dependence on the input motion (Shome et al., 1998).

Large percentage reductions often occur when a component produces substantial fixed-base drift but a more moderate isolated response. Conversely, when the fixed-base demand is already small, the numerical percentage improvement may be limited. Examining the absolute drift together with its paired percentage change provides a more balanced interpretation of these cases.

Comparisons across building heights require attention to the complete model configuration. The three frames differ in bay spacing, member sections, weight, and isolation design as well as story count. The results therefore describe the response of three distinct structural systems rather than an experiment in which height alone was varied. Although the nine-story configuration has the largest mean reduction in the present dataset, that observation should be read together with the differences in geometry and bearing design. A systematic height study would require those other features to be controlled.

For engineering assessment, the drift comparison provides an initial measure of how effectively the isolation arrangement limits relative floor deformation over a common earthquake suite. Complementary response quantities, including bearing displacement and floor acceleration, can be addressed in broader performance studies, as outlined in the next subsection.

5.6. Scope and Limitations

The first consideration concerns the elastic representation of the steel beams and columns. Although the models include geometric effects and nonlinear bearing response, the superstructures are not configured to simulate plastic hinge development, cyclic strength deterioration, local instability, or connection fracture. The reported drift demands should accordingly be interpreted for the specified elastic-member models. This assumption keeps the comparison focused on changes in elastic superstructure deformation associated with the isolation layer. It is therefore appropriate for the stated drift objective, while defining the boundary of the conclusions that can be drawn from the numerical results.

The second consideration is the selected response measure. Each earthquake contributes the maximum interstory drift observed anywhere in the superstructure, without a corresponding story-by-story drift envelope or simultaneous assessment of floor accelerations and bearing travel. Those additional measures would extend the analysis beyond the intended peak-drift comparison.

The third consideration involves differences between frame configurations. The SFP bearings were designed separately for each model, and the isolated cases include a moving base slab. Thus, the results compare complete fixed-base and isolated systems rather than isolating the independent effects of friction, surface curvature, or building height. A dedicated parametric study would be needed to separate these influences.

The findings are based on the response of the investigated steel frames to the FEMA P695 far-field suite and are limited to their peak interstory drift demand. Assessment of additional performance objectives, including collapse resistance and seismic performance factors, lies outside this study's defined scope.

6. Conclusion

This study evaluated peak interstory drift in steel moment-frame models with 3, 6, and 9 stories, comparing fixed-base and single friction pendulum isolated configurations under the same 44 horizontal components of the FEMA P695 far-field ground-motion suite. The paired analysis provides a consistent basis for quantifying the influence of the isolation layer on superstructure deformation. The main findings of the paper are listed as follows:

- Every reported paired comparison showed a lower maximum interstory drift in the isolated model. The mean record-wise reductions were 51.62% for the three-story frame, 51.80% for the six-story frame, and 55.59% for the nine-story frame, demonstrating a consistent direction of improvement over the selected components. The agreement of the paired results in the direction of change is reflected in both the record-by-record charts and the summary tables. The amount of improvement differs among components, but the observed overall trend remains favorable for the isolated configurations.
- The medians reinforce this trend, decreasing from 1.118% to 0.527% for the three-story frame, from 1.030% to 0.427% for the six-story frame, and from 1.004% to 0.354% for the nine-story frame. The sample standard deviation was also smaller after isolation in every case, indicating a reduction in the observed spread of peak drift demand.
- The amount of improvement nevertheless depended on the earthquake component: the smallest reductions were approximately 5–10%, whereas the largest exceeded 80%. The grouped record charts provide the corresponding absolute demands and show how individual motions contribute to the summary statistics.
- The nine-story model produced the largest mean record-wise reduction, reflecting the combined response of its structural and isolation properties. Since the configurations vary in more than story count, the comparative results are most appropriately interpreted for each complete modeled system.

Overall, the investigated SFP arrangements limited superstructure drift across the selected earthquake components. The analysis provides a basis for considering friction pendulum isolation as a drift-control strategy in the examined elastic steel frames and for extending future studies to additional response measures.

Data statement

Data will be made available upon reasonable request.

Conflict of Interest

The authors declare that there is no conflict of interest regarding the publication of this paper.

7. References

Almazán, J. L., & De la Llera, J. C. (2002). Analytical model of structures with frictional pendulum isolators. *Earthquake Engineering & Structural Dynamics, 31*(2), 305–332.

Almazán, J. L., De la Llera, J. C., & Inaudi, J. A. (1998). Modelling aspects of structures isolated with the frictional pendulum system. *Earthquake Engineering & Structural Dynamics, 27*(8), 845–867.

Buckle, I. G., & Mayes, R. L. (1990). Seismic isolation: History, application, and performance—A world view. *Earthquake Spectra, 6*(2), 161–201.

Constantinou, M. C., Mokha, A., & Reinhorn, A. M. (1990). Teflon bearings in base isolation II: Modeling. *Journal of Structural Engineering, 116*(2), 455–474.

Deringöl, A. H., & Güneyisi, E. M. (2019). Effect of friction pendulum bearing properties on behaviour of buildings subjected to seismic loads. *Soil Dynamics and Earthquake Engineering, 125*, 105746.

Federal Emergency Management Agency. (2009). *Quantification of building seismic performance factors (FEMA P695)*. Federal Emergency Management Agency.

Fenz, D. M., & Constantinou, M. C. (2006). Behaviour of the double concave Friction Pendulum bearing. *Earthquake Engineering & Structural Dynamics, 35*(11), 1403–1424.

Jangid, R. S. (2005). Optimum friction pendulum system for near-fault motions. *Engineering Structures, 27*(3), 349–359.

Jangid, R. S., & Datta, T. K. (1995). Seismic behavior of base-isolated buildings: A state-of-the-art review. *Proceedings of the Institution of Civil Engineers – Structures and Buildings, 110*(2), 186–203.

Kelly, J. M. (1999). The role of damping in seismic isolation. *Earthquake Engineering & Structural Dynamics, 28*(1), 3–20.

Kitayama, S., & Cilsalar, H. (2022). Seismic loss assessment of seismically isolated buildings designed by the procedures of ASCE/SEI 7-16. *Bulletin of Earthquake Engineering, 20*, 1143–1168.

Kitayama, S., & Constantinou, M. C. (2018). Collapse performance of seismically isolated buildings designed by the procedures of ASCE/SEI 7. *Engineering Structures, 164*, 243–258.

Matsagar, V. A., & Jangid, R. S. (2008). Base isolation for seismic retrofitting of structures. *Practice Periodical on Structural Design and Construction, 13*(4), 175–185.

McKenna, F. (2011). OpenSees: A framework for earthquake engineering simulation. *Computing in Science & Engineering, 13*(4), 58–66.

Mokha, A., Constantinou, M. C., & Reinhorn, A. M. (1990). Teflon bearings in base isolation I: Testing. *Journal of Structural Engineering, 116*(2), 438–454.

Mokha, A., Constantinou, M. C., Reinhorn, A. M., & Zayas, V. A. (1991). Experimental study of friction-pendulum isolation system. *Journal of Structural Engineering, 117*(4), 1201–1217.

Mosqueda, G., Whittaker, A. S., & Fenves, G. L. (2004). Characterization and modeling of friction pendulum bearings subjected to multiple components of excitation. *Journal of Structural Engineering, 130*(3), 433–442.

Naeim, F., & Kelly, J. M. (1999). *Design of seismic isolated structures: From theory to practice*. John Wiley & Sons.

Shome, N., Cornell, C. A., Bazzurro, P., & Carballo, J. E. (1998). Earthquakes, records, and nonlinear responses. *Earthquake Spectra, 14*(3), 469–500.

Warn, G. P., & Ryan, K. L. (2012). A review of seismic isolation for buildings: Historical development and research needs. *Buildings, 2*(3), 300–325.

Zayas, V. A., Low, S. S., & Mahin, S. A. (1990). A simple pendulum technique for achieving seismic isolation. *Earthquake Spectra, 6*(2), 317–333.

Zhu, M., McKenna, F., & Scott, M. H. (2018). OpenSeesPy: Python library for the OpenSees finite element framework. *SoftwareX, 7*, 6–11.

Appendix A. Record-level peak drift results

Table A1 lists the peak interstory drift values used to construct Figure 1. For each horizontal component, the table gives the fixed-base and SFP-isolated results for all three frame heights. The values represent building-level maxima over the corresponding response history.

Table A1. Peak interstory drift ratios (%) in the 44 paired records for each frame.

Record	3-story FB	3-story SFP	6-story FB	6-story SFP	9-story FB	9-story SFP
01	3.188	0.763	2.064	0.563	1.613	0.422
02	3.070	0.608	2.203	0.551	1.486	0.475
03	1.110	0.593	0.918	0.432	1.534	0.347
04	1.981	0.623	1.042	0.653	0.733	0.432
05	2.250	0.588	1.255	0.482	1.490	0.382
06	3.499	0.579	1.805	0.697	1.839	0.428
07	1.374	0.460	1.171	0.426	0.581	0.416
08	1.410	0.474	1.695	0.404	0.990	0.549
09	0.686	0.514	0.562	0.428	0.796	0.378
10	1.367	0.539	1.046	0.424	1.004	0.434
11	0.819	0.396	1.022	0.363	1.087	0.370
12	0.878	0.502	0.916	0.479	0.709	0.319
13	0.939	0.555	0.902	0.427	1.191	0.317
14	0.942	0.581	0.798	0.517	1.064	0.299
15	1.126	0.593	1.058	0.460	0.919	0.309
16	0.807	0.538	0.851	0.404	0.705	0.328
17	1.420	0.438	0.839	0.380	1.723	0.640
18	2.066	0.490	2.260	0.427	1.674	0.447
19	0.356	0.314	0.312	0.270	0.243	0.194
20	0.353	0.332	0.479	0.368	0.389	0.352
21	1.490	0.595	1.849	0.403	1.078	0.564
22	1.071	0.476	1.112	0.458	0.581	0.314
23	0.617	0.535	0.536	0.394	0.464	0.303

Record	3-story FB	3-story SFP	6-story FB	6-story SFP	9-story FB	9-story SFP
24	1.082	0.596	1.663	0.552	0.870	0.325
25	1.663	0.533	2.294	0.468	0.831	0.514
26	0.907	0.693	0.914	0.497	0.598	0.350
27	0.809	0.439	0.661	0.404	0.433	0.310
28	1.279	0.492	1.334	0.368	1.497	0.378
29	1.018	0.521	0.772	0.406	1.420	0.334
30	1.712	0.478	1.321	0.407	2.101	0.382
31	1.165	0.522	1.397	0.397	1.089	0.322
32	0.860	0.456	1.039	0.404	1.590	0.392
33	1.169	0.487	1.106	0.458	1.004	0.280
34	0.985	0.468	0.799	0.379	1.064	0.275
35	1.807	0.571	1.395	0.609	1.006	0.429
36	1.353	0.480	1.107	0.431	0.584	0.346
37	1.545	0.550	0.921	0.611	1.688	0.730
38	2.558	0.867	1.353	1.040	2.968	1.586
39	0.870	0.559	0.741	0.391	0.542	0.368
40	1.367	0.628	0.820	0.535	1.016	0.347
41	0.790	0.452	0.966	0.422	0.530	0.356
42	0.407	0.352	0.258	0.245	0.584	0.283
43	0.791	0.375	0.632	0.341	0.460	0.253
44	1.000	0.626	0.659	0.506	0.475	0.250

FB denotes fixed-base, and SFP denotes single friction pendulum isolation. The component order follows Figure 1 and the response-history dataset.